Original Research

Hyperpolarized Choline as an MR Imaging Molecular Probe: Feasibility of In Vivo Imaging in a Rat Model

Lanette J. Friesen-Waldner, PhD,[1] Trevor P. Wade, PhD,[1,2] Kundan Thind, PhD,[1,2] Albert P. Chen, PhD,[3] J. Moshe Gomori, MD,[4] Jacob Sosna, MD,[4] Charles A. McKenzie, PhD,[1,2] and Rachel Katz-Brull, PhD[4,5]*

Purpose: To assess the feasibility of choline MRI using a new choline molecular probe for dynamic nuclear polarization (DNP) hyperpolarized MRI.

Materials and Methods: Male Sprague-Dawley rats with an average weight of 400 ± 20 g (n = 5), were anesthetized and injection tubing was placed in the tail vein. [1,1,2,2-D_4, 1-^{13}C]choline chloride (CMP1) was hyperpolarized by DNP and injected into rats at doses ranging from 12.6 to 50.0 mg/kg. Coronal projection ^{13}C imaging was performed on a 3 Tesla clinical MRI scanner (bore size 60 cm) using a variable flip angle gradient echo sequence. Images were acquired 15 to 45 s after the start of bolus injection. Signal intensities in regions of interest were determined at each time point and compared.

Results: ^{13}C MRI images of hyperpolarized CMP1 at a 50 mg/kg dose showed time-dependent organ distribution patterns. At 15 s, high intensities were observed in the inferior vena cava, heart, aorta, and kidneys. At 30 s, most of the signal intensity was localized to the kidneys. These distribution patterns were reproduced using 12.6 and 25 mg/kg doses. At 45 s, only signal in the kidneys was detected.

Conclusion: Hyperpolarized choline imaging with MRI is feasible using a stable-isotope labeled choline analog (CMP1). Nonradioactive imaging of choline accumulation may provide a new investigatory dimension for kidney physiology.

Key Words: choline; metabolism; magnetic resonance imaging
J. Magn. Reson. Imaging 2014;00:000–000.

CHOLINE IS AN essential nutrient that is found at the metabolic crossroad of lipid synthesis, one carbon metabolism, and neurotransmitter metabolism. (1) Because it is an essential component in cell membrane synthesis, choline is important in cell cycle progression, proliferation, and apoptosis, processes that are disturbed in malignant cells and tumors. (2) Positron emission tomography (PET) imaging of choline has been shown to be highly specific in the detection of hepatocellular carcinoma, (3) prostate cancer, (4) breast cancer, (5) and gynecologic tumors. (6)

Choline uptake by the kidneys is a physiological process that has important implications, such as (i) the ability to recruit compounds that are converted to kidney osmolytes (betaine and glycerophosphocholine) (7) and thereby offer protection against various stress factors, and (ii) the ability to protect the subject from cholinergic intoxication.

The clinical implications of the ability to image choline uptake in kidneys are potentially important, and could include the ability to provide quantitative measurement of each kidney function individually and noninvasively. For this reason, the ability to monitor and quantify choline uptake in the kidney is likely to provide a new, noninvasive tool for investigating important factors related to kidney physiology.

Based on prior studies, the rate of choline uptake in healthy kidneys is likely comparable to the rate in cancer cells: A kidney uptake mechanism with a K_m of 80–155 μM and a V_{max} of 71 pmol/μL water cell/min was previously reported. (8) Assuming the kidney contains approximately 85% water, this rate can be expressed as *ca.* 61 nmol/min/g. In breast cancer

[1]Department of Medical Biophysics, The University of Western Ontario, London, Ontario, Canada.
[2]Robarts Research Institute, The University of Western Ontario, London, Ontario, Canada.
[3]GE Healthcare.
[4]Department of Radiology, Hadassah-Hebrew University Medical Center, Jerusalem, Israel.
[5]BrainWatch Ltd, Tel-Aviv, Israel.

Additional Supporting Information may be found in the online version of this article.

Drs. Friesen-Waldner and Wade contributed equally to this work.

Drs. McKenzie and Katz-Brull contributed equally to this work.

Contract grant sponsor: Israel Science Foundation; Contract grant number: 284/10.

*Address reprint requests to: R.K.-B., Department of Radiology, Hadassah-Hebrew University Medical Center, Ein-Kerem, Jerusalem, Israel 91120. E-mail: rkb@hadassah.org.il

Received January 31, 2014; Accepted April 2, 2014.
DOI 10.1002/jmri.24659
View this article online at wileyonlinelibrary.com.

cells, a maximal choline uptake rate of 20 nmol/mg protein/h was previously described. (9) The amount of protein in these cells was 220 pg protein/cell. Therefore, taking into account *ca.* 10^9 cells per 1 g of tumor tissue, the maximal rate of choline transport in breast cancer is estimated to be *ca.* 73 nmol/min/g, which is similar to the uptake rate reported in the kidney.

Thus, in the process of developing an MRI choline molecular probe that can demonstrate tissue choline uptake, a proof of principle in healthy rat kidneys may provide an indication for the feasibility of this approach for imaging choline uptake in cancer tumors as well.

Recent advances in hyperpolarized MRI (10) have enabled in vivo observation of signal from ^{15}N and ^{13}C labeled small compounds at 3–4 orders of magnitude above thermal equilibrium signal-to-noise ratio. (11) The spin-lattice relaxation time (T_1) of the reporting nucleus in the molecular probe limits the temporal window at which hyperpolarized MRI images can be acquired. Normally, MR images or spectra of a hyperpolarized compound will be acquired within approximately three times the T_1 of the reporting nucleus. ^{15}N-choline has a favorable T_1 (*ca.* 2 min) for hyperpolarized imaging. (12) However, ^{15}N transmission and RF circuits are not available on most clinical scanners. Deuteration of the methylene positions in the choline molecule was previously shown to lead to T_1 prolongation of these methylene carbon positions (*ca.* 1 min at 37°C and 7T) (13) which consequently enabled ^{13}C-MR studies of hyperpolarized choline. (14,15) Most hyperpolarized MR studies of choline have focused on the metabolic fates of hyperpolarized choline in vitro. (14–16) Here, the metabolic fate of the choline molecular probe was not of interest per se; instead the aim was to illustrate that a hyperpolarized choline probe could be reliably detected in vivo. Thus, the aim of this study was to test the feasibility of imaging a carbon-13 enriched choline molecular probe using hyperpolarized MRI.

MATERIALS AND METHODS

Materials

[1,1,2,2-D_4, 1-^{13}C]choline chloride (CMP1) was contributed by BrainWatch Ltd. (BW-41, BrainWatch Ltd., Tel-Aviv, Israel). Trityl free radical (OX063) was obtained from GE Healthcare, (London, UK). ProHance was purchased from Bracco Diagnostics Inc. (USA). Atropine was obtained from Sigma-Aldrich (Canada).

Animals

All studies were performed under a protocol approved by the local institution's Animal Care and Use Committee. Male Sprague-Dawley rats, 400 ± 20 g ($n = 5$) (corresponding to an average age of approximately 14 weeks (17)), were acclimated for a week before the study. The rats were fed ad libitum. Anesthesia was induced with 5 % isoflurane and maintained with 1.5 to 2.5 % isoflurane. Fifteen minutes before choline injection, the rats were given atropine intravenously at a dose of 1 mg/kg to avoid adverse cholinergic effects. Hyperpolarized media were injected by means of a tail vein catheter prewashed with heparinized saline, in a 12 s bolus (2.5 mL) for each experiment. The injected CMP1 dose was 12.6, 25.0, 40.0, or 50.0 mg/kg. Following the hyperpolarized studies, the rats were killed by isoflurane overdose and intravenous injection of potassium chloride.

Hyperpolarization and Dissolution

A typical composition of the polarization solution consisted of: CMP1 (27.3 mg, 0.189 mmol) mixed with 7.1 mg of an aqueous solution of OX063 (61 mM) and ProHance (2.9 mM). The contrast agent ProHance was added to the preparation as it was previously shown that the addition of a Gd-complex to the solid-state preparation increases the polarization level reached at 3.35T. (18) Because different Gd-complexes may differ in their effect on specific probes, (19) ProHance was used here for consistency with the hyperpolarization protocol for choline chloride that was previously found beneficial. (13–15,20) The polarization solution was hyperpolarized in a dissolution DNP polarizer (Hypersense, Oxford Instruments, Abingdon, UK) at 1.4 K, 94.1 GHz, and 50 mW. Polarization build-up data are provided in the Supplementary Information, which is available online.

Dissolution was performed in 4 mL of dissolution medium containing sodium chloride and 100 mg/liter EDTA. The amount of CMP1 in the polarization solution was calculated to provide the intended CMP1 dose (12.6, 25, or 50 mg/kg) when 2.5 mL out of 4 mL of a hyperpolarized CMP1 solution (the dissolution medium containing the hyperpolarized CMP1) was injected into a specific rat (with a specific weight). Thus, the amount of CMP1 was calculated per animal per dose. The amount of sodium chloride in the dissolution medium was calculated to complement the final CMP1 concentration in the hyperpolarized CMP1 solution to obtain 300 mOsm. A 2.5 mL volume of the 12.6, 25, or 50 mg/kg hyperpolarized CMP1 solutions was administered to the rats by means of tail vein bolus injection, starting 20–25 s after the start of dissolution.

Determination of T_1 for CMP1 at 3 Tesla

T_1 measurements in a hyperpolarized state consisted of recording the decay curve of the hyperpolarized signal at a temporal resolution of 1 s. The effect of radiofrequency (RF) pulsation ($\theta = 10°$) on the decay rate was taken into account using a point-by-point correction of the data by a factor of $1/\cos(\theta)$. These corrected intensity data were analyzed using the standard decay equation, i.e., $S_t = S_i * \exp(-t/T_1)$, where S_t is the signal at each time point, t, (corrected for the effect of flip angle of the preceding pulse), and S_i is the signal in the 1st spectrum (i.e., before pulsation and T_1 decay during the measurement. The flip angle of 10° was chosen to provide sufficient signal for analysis of single spectra yet use only a small portion

of the polarization per transient, to allow monitoring of the decay curve at high temporal resolution. Curve fitting was carried out using Matlab software (The MathWorks Inc., Natick, MA).

MR Imaging

MRI was performed in a 3 Tesla (T) clinical MRI scanner (Discovery MR 750, GE Healthcare, Waukesha, WI), equipped with a transmit/receive birdcage ^{13}C RF coil (85 mm diameter, 120 mm long, 8 rung, low-pass with less than 20% variation in B_1 over a central region 50 mm in diameter by 80 mm long) and a custom built transmit/receive ^{1}H surface coil (70 mm long, 50 mm wide) that fits within the ^{13}C coil. The animal was placed in a supine position at the center of the ^{13}C coil and the proton coil was centered underneath its abdomen. Proton T_1-weighted images were acquired for anatomical localization. Variations in anatomical coverage resulted from variations in positioning of the rat with respect to the proton RF coil.

Coronal projection ^{13}C imaging was performed using a variable flip angle gradient echo sequence(21) with the following acquisition parameters: acquisition time 1 s, 200 μs nonselective RF hard pulse, repetition time (TR) 17.7 ms, echo time (TE) 8.9 ms, readout bandwidth ± 2.0 kHz, centric phase encoding, matrix size 64 × 64, field-of-view (FOV) 200 × 200 mm. The variable flip angle scheme was designed to consume 99% of the polarization by the end of the acquisition. Images were acquired 15, 30, or 45 s after the start of the bolus injection of the hyperpolarized CMP1 solution. Up to three injections of hyperpolarized CMP1 were performed in each animal. For each injection, a single CMP1 dose was used and one image was acquired at a single time point.

Regions of interest (ROIs) were drawn in the heart, liver, and kidneys (T.W., 10 years of experience). The signal intensities in these ROIs, in the images recorded at various times after injection of various choline doses were assessed and compared.

RESULTS

Hyperpolarized CMP1 imaging in anesthetized rats showed the distribution of CMP1 in the vasculature, heart, kidneys, and liver (Fig. 1). The head, neck, and tail were outside the field-of-view and the sensitive region of the ^{13}C RF coil. ^{13}C signal distribution depended on the time between the start of the bolus injection and the image recording, whereas the duration of the bolus injection was 12 s. The signal observed at 15 s showed high intensity in the inferior vena cava, heart, aorta, and kidneys, and low intensity in the liver (Figs. 1a, 2a). At 30 s, the heart and vasculature signal were greatly reduced, the kidney signal increased, and the liver remained low (Figs. 1b, 2a). A second image from a different rat, recorded at the same time and dose (Fig. 1e), demonstrated a similar image pattern. The signal characteristics of the two images were analyzed (Fig. 2b) and found comparable.

It should be noted that because each image was acquired following a separate hyperpolarized CMP1 bolus, image intensities were not normalized to the polarization of the substrate in solution and image intensities are reported in arbitrary raw data units. Nevertheless, polarization in the solid state (determined in arbitrary polarizer units) were similar from one polarization to another (per dose) and images of different rats acquired under similar conditions yielded similar intensities.

A typical image acquired 45 s after injection is shown in Figure 1c. The ^{13}C signal in the kidneys at this time point was higher in intensity than the signal at any other location, but 57 % lower (in arbitrary signal units, Fig. 2a) than the signal at 30 s.

The dose effect in CMP1 studies was explored using two tests. In the first test, image acquisition was at 15 s from the start of the CMP1 injection and the dose was 12.6 mg/kg (Fig. 1f), roughly one fourth of the 50 mg/kg dose described above (Fig. 1d). At the lower dose, the signal was again observed in the inferior vena cava, heart, aorta, and kidneys, and at low intensity in the liver. However, while the high dose injection produced a kidney signal that was 1.5-fold higher than signal in the heart, signal intensities in the kidneys and heart were similar in the low dose study, with mean kidney-to-heart signal ratio of 0.9 (n = 1) (Fig. 2c).

In the second test, image acquisition was at 30 s, with a CMP1 dose of 25 mg/kg, half the original dose (Fig. 1g). Signal distribution features at this time point were similar at 50 and 25 mg/kg; the kidney signal predominated and the liver signal was lower but visible. The kidney-to-liver signal intensity ratio was 2.4 (n = 2) at 25 mg/kg and 3.8 (n = 1) at 50 mg/kg.

DISCUSSION

We have shown here for the first time, images of choline distribution in real-time using a noninvasive, radiation-free imaging modality. Hyperpolarized choline imaging was found to be tissue specific and to vary with time.

An increase in the absolute ^{13}C signal intensity in the kidney was observed at 30 s compared with 15 s after the onset of the bolus injection. This increase in signal over time was surprising and counter intuitive as one would expect a T_1 relaxation-induced signal decrease. A possible explanation for the higher signal intensity in the kidneys at 30 s is the choline transport mechanism efficiency in the kidney, leading to a higher actual level of hyperpolarized choline in the kidney at 30 s versus 15 s. Additional choline signal observed in the kidney at 30 s has likely not arrived at the kidneys at 15 s. At 15 s, some of the choline was still in the heart and main vessels, and a part may have lingered in the tail vein after injection.

A decrease in the ^{13}C signal intensity in the kidney was observed at 45 s compared with 30 s. Assuming the polarization of the substrate and its uptake rate

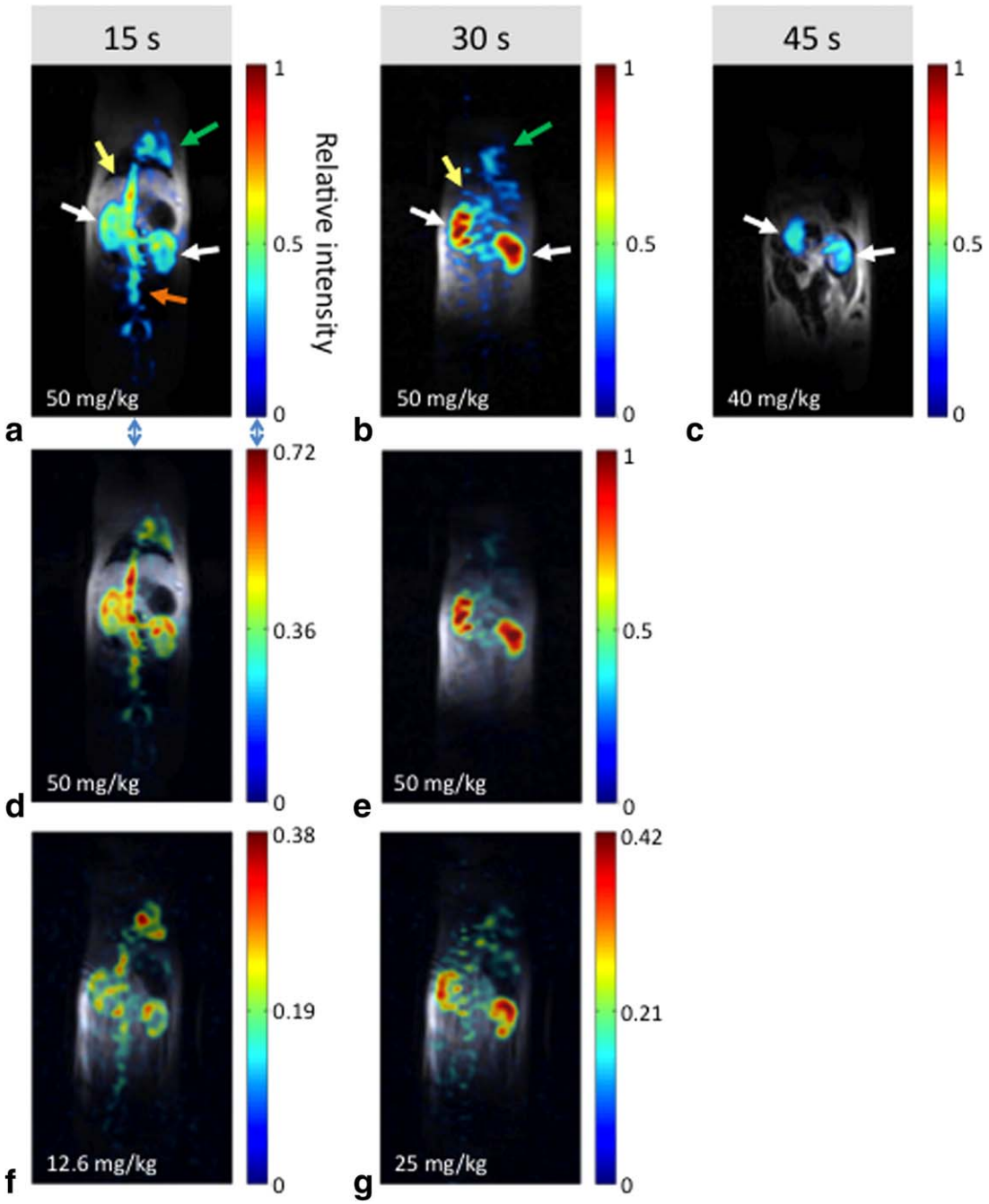

Figure 1. ^{13}C MRI body images of rats injected with hyperpolarized [1,1,2,2-D_4, 1-^{13}C]choline chloride (CMP1). The signal in these images represents the total ^{13}C signal. Variations in signal distribution are shown at various time points from the start of the bolus and following various CMP1 doses. Color hyperpolarized projection images are digitally fused to proton images from the same rat to confirm the anatomical locations of the ^{13}C signal. The color scales represent relative arbitrary linearly distributed ^{13}C intensity units for the hyperpolarized images. Relative intensities within and between the color images can be compared based on the corresponding value in the color scale. Each image is presented with the optimal viewing window for demonstration of the temporal and dose effects discussed in the text. Image **a**†was recorded 15 s after bolus initiation with a dose of 50 mg/kg in rat #1. Image **b** was recorded 30 s after bolus initiation with a dose of 50 mg/kg in rat #2. Image **c** was recorded 45 s after bolus initiation with a dose of 40 mg/kg in rat #3. Image **d** was recorded 15 s after bolus initiation with a dose of 50 mg/kg in rat #1. This is the same image as in a, presented with a different viewing window for ease of visual comparison. Image **e** was recorded 30 s after bolus initiation with a dose of 50 mg/kg in rat #4. Image **f** was recorded 15 s after bolus initiation with a dose of 12.6 mg/kg in rat #5. Image **g** was recorded 30 s after bolus initiation with a dose of 25 mg/kg in rat #5. The bolus volume and duration were *ca.* 2.5 mL and 12 s, respectively, for all injections. CMP1 was administered by means of the tail vein. Image recording time was 1 s. The head and tail regions were outside the field-of-view for both the ^{1}H and ^{13}C RF coils. †The kidneys, inferior vena cava, heart, and liver region are marked with white, orange, green, and yellow arrows, respectively.

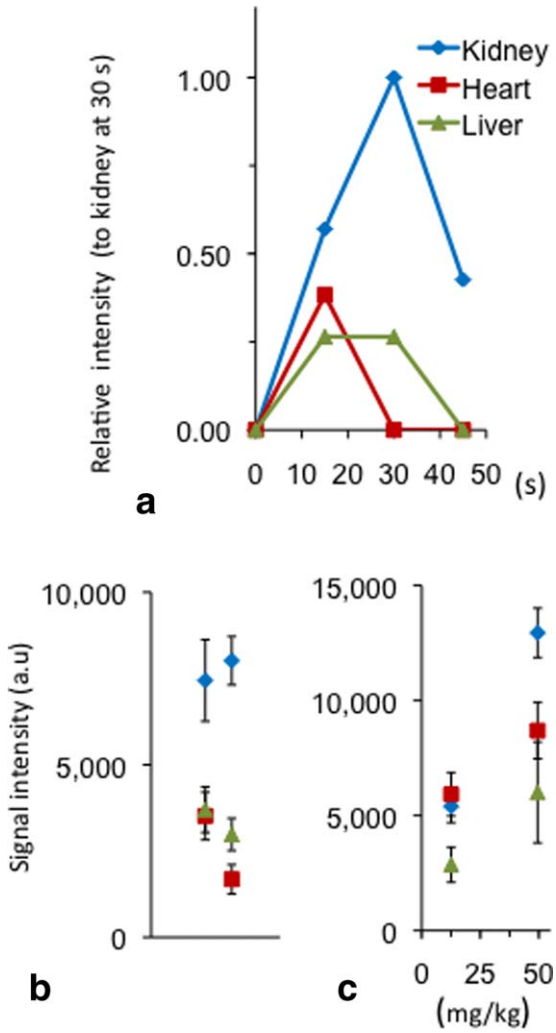

Figure 2. Signal intensity in kidney, heart, and liver on ^{13}C MRI body images of rats injected with hyperpolarized CMP1. **a:** Temporal behavior of the hyperpolarized signal in the kidney, heart, and liver following injection of a high CMP1 dose injection. The maximal relative intensities are shown and correspond to Figures 1a, 1b, and 1c. Lines connecting the various time points are drawn for visualization of general trends. **b:** Reproducibility of signal intensities in 2 images acquired in two different rats, both injected with a dose of 25 mg/kg and imaged 30 s after the start of injection. Raw signal intensities in arbitrary units are presented as mean ± standard deviation of the signal in the region of interest drawn in each organ. **c:** Organ distribution of hyperpolarized CMP1 at 15 s after the start of injection of 12.6 and 50 mg/kg. These relative and raw signal intensities in this figure were not manipulated and specifically were not corrected for polarization or relaxation.

were the same for these two experiments, we may assume that this decrease in arbitrary signal units represents an actual decrease in the signal intensity in the kidneys (rather than a decrease in choline content). Considering a signal decrease due to T_1 relaxation during the 15 s delay in image acquisition as well as the lower, inadvertent, CMP1 dose used in the image acquired at 45 s, the expected signal decrease is ~60%, which agrees with the experimental result (57%).

This type of analyses demonstrated the potentially direct and quantitative nature of hyperpolarized choline imaging.

By varying the injected dose of hyperpolarized CMP1 we showed that kidney-to-heart signal ratio, determined 15 s after the start of injection (3 seconds after the end of bolus injection), was 1.7-fold higher in a 50 mg/kg dose compared with a dose approximately fourfold lower. This finding suggested that the kidney accumulated more choline at the higher dose. By reducing the injected hyperpolarized CMP1 dose twofold and imaging later in time, at 30 s, the kidney-to-liver signal ratio was found to decrease. This signal ratio was 1.6-fold higher in a 50 mg/kg dose compared with the lower dose. This finding also suggested higher accumulation of CMP1 in the kidney at the higher dose. This initial investigation into the time and dose dependent characteristics of hyperpolarized CMP1 imaging in the kidney suggested that hyperpolarized choline MRI may enable assessment of kidney function.

Although the liver is known for its ability to accumulate choline, (22,23) only a low label level was observed in the liver. In a PET study that used ^{11}C-enriched choline, liver accumulation was not observed until approximately 5 min after choline injection, with a gradual increase until maximum signal intensity was seen at approximately 35 min after injection. (24) These time frames (5–35 min) are clearly not attainable with hyperpolarized CMP1 due to the relatively fast decay of hyperpolarized media (T_1 ~39 s in blood at 37°C and 14.1T, (14) and up to 70 s for ^{13}C in general, comparable to observation windows of 2–3.5 min), compared with *ca.* 20 min ^{11}C half-life. Further studies may aid in characterizing the time course for hyperpolarized CMP1 uptake in the liver. In the current study, the relatively low liver signal disappeared by 45 s, most likely due to T_1 relaxation.

Kidney and liver signal accumulation is in general agreement with kinetic rate constants for choline uptake that were previously determined in these organs. As described in the introduction, the kidney maximal choline uptake rate is approximately 61 nmol/min/g. In rat liver cells, an uptake mechanism with a K_m of 340 μM and a V_{max} of 0.45 nmol/mg protein/15 s was reported.(25) Using a previously determined conversion factor of 21 mg protein/g tissue,(26) the choline uptake V_{max} in the liver can be expressed as 38 nmol/min/g. Thus the maximal rate of choline uptake in the liver is two-thirds that of the kidney, and the affinity of the liver choline transport system is approximately twofold lower.

K_m values in the kidney and liver represent the availability of intermediate- and low-affinity choline transporters in various tissues (27); other choline transporters can be found in the blood-brain barrier, cancer cells (low to medium affinity), (9,28,29) and cholinergic neurons (high affinity). From the above kinetic rate constants in the kidney and liver, it would appear that at normal physiological concentrations of choline (between 10 and 100 μM) as well as at the high doses used here in the hyperpolarized studies (estimated initial level in the blood > 1 mM), choline

uptake would occur primarily in the kidney, where hyperpolarized CMP1 levels would be roughly twice those of the liver. The findings in our experiments are consistent with these expectations; the kidney-to-liver signal ratio was 2.4 at 30 s following a 25 mg/kg injection. The 1.6 higher kidney-to-liver signal ratio following a 50 mg/kg dose may indicate the observation of kidney choline uptake mechanisms in vivo that are of higher efficiency than previously reported.

CMP1 signal was observed in the heart 15 s after the start of injection; however, this signal appears to represent hyperpolarized CMP1 in blood and not myocardial uptake, because it is much reduced at 30 s and disappears at 45 s, along with the CMP1 signal in the major blood vessels. We note that heart anatomy cannot be discerned in these images because the imaging time (1s) averaged approximately six heart beats.

CMP1 is labeled with four deuterium atoms. Chemically, deuterium behaves similarly to ordinary hydrogen. However, for compounds of heavy hydrogen isotopes there are differences in bond energy and length that are larger than the isotopic differences in any other element. Deuterium-carbon bonds are somewhat stronger than corresponding hydrogen bonds, and these differences may lead to changes in specific biological reactions. Interestingly, the same deuteration strategy used in CMP1 was recently described for a radioactive PET-choline agent - [^{18}F]fluoro-[1,2-$^{2}H_4$]choline. (30) With this choline analog, uptake profiles revealed reduced uptake in the heart, lung, and liver for deuterated choline analogs. These findings appear similar to the pattern observed in the current study, with heart and lung uptake undetected and liver uptake low, although in line with the previous cellular characterization described above in terms of maximal rates.

It was previously shown for a similar choline molecular probe, [1,1,2,2-D_4, 2-^{13}C]choline chloride (CMP2), that changes in magnetic field strength had little or no effect on the T_1 of the labeled ^{13}C position. (14) In addition, at 14.1T there was only a 17% shortening in T_1 in whole blood compared with an isotonic solution. (14) It was, therefore, concluded that a lower limit for CMP2 T_1 in vivo (in blood) would be ~39 s. The current measurement of CMP1 T_1 in solution at 3T showed a slightly lower value than expected (30 s, Supplementary Information). Nevertheless, the feasibility of using this molecular probe for hyperpolarized MRI imaging has been demonstrated.

In the past decade, radioactively labeled choline analogs (^{11}C-choline and ^{18}F-choline) have been used to track and identify tumors using PET. (31) While PET has high sensitivity and spatial resolution for cancer imaging, hyperpolarized ^{13}C-choline MRI has the potential to provide additional information such as the ability to inspect rapid uptake of choline. In addition, hyperpolarized MRI has the potential to provide information regarding metabolic fluxes through observation of the metabolic by-products of choline. The hyperpolarized ^{13}C-choline method provides complementary information to PET and may offer an alternative to PET where the use of ionizing radiation cannot be justified, for example in some populations (e.g., pregnant women, children) and in repeated studies.

We note that neither urinary bladder nor urine were labeled during the time frame during which signal was observed in the kidneys. This is an important consideration if CMP1 is to be used for studies of prostatic cancer, as signal from the bladder and/or urine may mask the choline signal in the proximal prostate.

Choline chloride is toxic at high doses as a potentially acute cholinergic intoxication agent. Previous investigation showed no toxic effects in mice in doses up to 21.5 mg/kg but did find toxic effects at a dose of 53 mg/kg. (32) For this reason, the rats in the current study were given atropine—to protect them from acute cholinergic intoxication. Further study of choline chloride toxicity is required. In addition, development of less toxic derivatives of choline such as CDP-choline (32) for hyperpolarized MRI may be warranted as well.

This study had several limitations: (i) projection images were acquired rather than slice selective acquisitions. Slice selective and 3D total ^{13}C imaging of hyperpolarized substrates is under development; (ii) the images did not cover the entire animal and thus important information on choline uptake in the head and neck region is missing. ^{13}C RF coils with larger coverage are under development in our group for this purpose; (iii) only one carbon position in the choline molecular probe was labeled with ^{13}C. Choline contains five carbon positions and thus a fully ^{13}C labeled, fully deuterated choline molecular probe may have provided higher imaging signal. This strategy was recently used for obtaining the first nonradioactive images of glucose distribution in vivo, (33) where we used a fully ^{13}C labeled, fully deuterated glucose analog. Thus, further studies with such a choline analog are warranted, but would require custom synthesis of this choline analog as it is not available commercially.

In conclusion, imaging of hyperpolarized choline in vivo is feasible. Based on the findings presented here, it is shown that choline uptake by the kidney may be quantified and it is possible that the results described here may be relevant for cancer imaging as well. The ability to image hyperpolarized choline by MRI is promising as an extension to ^{11}C- or ^{18}F-choline-PET. Future studies will determine if the hyperpolarized choline approach will indeed prove useful in preclinical models of disease and then in clinical investigations.

ACKNOWLEDGMENTS

We thank Prof. Eugene Libson for support and useful discussions during the study. Rachel Katz-Brull is a shareholder of BrainWatch Ltd. J. Moshe Gomori is a consultant of BrainWatch Ltd. Albert Chen is an employee of GE Healthcare. This work was funded by BrainWatch Ltd. C.A.M. was funded by the Canada Research Chairs program, the Ontario Research Fund, and the Ontario Institute for Cancer Research. R.K.B. was funded by the Israel Science Foundation.

REFERENCES

1. Blusztajn JK. Choline, a vital amine. Science 1998;281:794–795.
2. Ridgway ND. The role of phosphatidylcholine and choline metabolites to cell proliferation and survival. Crit Rev Biochem Mol Biol 2013;48:20–38.

3. Salem N, Kuang Y, Wang F, MacLennan GT, Lee Z. PET imaging of hepatocellular carcinoma with 2-deoxy-2[F-18]fluoro-D-glucose, 6-deoxy-6[F-18]fluoro-D-glucose, [C1–11]-acetate and [N-methyl-C-11]-choline. Q J Nucl Med Mol Imaging 2009;53:144–156.
4. Awwad HM, Geisel J, Obeid R. The role of choline in prostate cancer. Clin Biochem 2012;45:1548–1553.
5. Contractor KB, Kenny LM, Stebbing J, et al. [C-11]Choline positron emission tomography in estrogen receptor-positive breast cancer. Clin Cancer Res 2009;15:5503–5510.
6. Torizuka T, Kanno T, Futatsubashi M, et al. Imaging of gynecologic tumors: comparison of C-11-choline PET with F-18-FDG PET. J Nucl Med 2003;44:1051–1056.
7. Burg MB. Molecular basis of osmotic regulation. Am J Physiol 1995;268(Pt 2):F983–F996.
8. Grunewald RW, Oppermann M, Muller GA. Choline transport and its osmotic regulation in renal cells derived from the rabbit outer medullary thick ascending limb of Henle. Pflugers Arch 1997;434:815–821.
9. Katz-Brull R, Seger D, Rivenson-Segal D, Rushkin E, Degani H. Metabolic markers of breast cancer: enhanced choline metabolism and reduced choline-ether phospholipid synthesis. Cancer Res 2002;62:1966–1970.
10. Ardenkjaer-Larsen JH, Fridlund B, Gram A, et al. Increase in signal-to-noise ratio of > 10,000 times in liquid-state NMR. Proc Natl Acad Sci U S A 2003;100:10158–10163.
11. Kurhanewicz J, Vigneron DB, Brindle K, et al. Analysis of cancer metabolism by imaging hyperpolarized nuclei: prospects for translation to clinical research. Neoplasia 2011;13:81–97.
12. Cudalbu C, Comment A, Kurdzesau F, et al. Feasibility of in vivo N-15 MRS detection of hyperpolarized N-15 labeled choline in rats. Phys Chem Chem Phys 2010;12:5818–5823.
13. Allouche-Arnon H, Lerche MH, Karlsson M, Lenkinski RE, Katz-Brull R. Deuteration of a molecular probe for DNP hyperpolarization – a new approach and validation for choline chloride Contrast Media Mol Imaging 2011;6:499–506.
14. Allouche-Arnon H, Gamliel A, Barzilay CM, et al. A hyperpolarized choline molecular probe for monitoring acetylcholine synthesis. Contrast Media Mol Imaging 2011;6:139–147.
15. Allouche-Arnon H, Gamliel A, Sosna J, Gomori JM, Katz-Brull R. In vitro visualization of betaine aldehyde synthesis and oxidation using hyperpolarized magnetic resonance spectroscopy. Chem Commun 2013;49:7076–7078.
16. Gabellieri C, Reynolds S, Lavie A, Payne GS, Leach MO, Eykyn TR. Therapeutic target metabolism observed using hyperpolarized N-15 choline. J Am Chem Soc 2008;130:4598–4599.
17. Taconic.com. Sprague-Dawley one year growth. Available at: http://www.taconic.com/SD. Accessed March 2014.
18. Ardenkjaer-Larsen JH, Macholl S, Johannesson H. Dynamic nuclear polarization with trityls at 1.2 K. Appl Magn Reson 2008;34:509–522.
19. Friesen-Waldner L, Chen A, Mander W, Scholl TJ, McKenzie CA. Optimisation of dynamic nuclear polarisation of 1-C-13 pyruvate by addition of gadolinium-based contrast agents. J Magn Reson 2012;223:85–89.
20. Allouche-Arnon H, Hovav Y, Friesen-Waldner L, et al. Quantification of rate constants for successive enzymatic reactions with DNP hyperpolarized MR. NMR Biomed 2014. (in press).
21. Santyr GE, Lam WW, Ouriadov A. Rapid and efficient mapping of regional ventilation in the rat lung using hyperpolarized 3He with Flip Angle Variation for Offset of RF and Relaxation (FAVOR). Magn Reson Med 2008;59:1304–1310.
22. Kuang Y, Salem N, Tian HB, et al. Imaging Lipid synthesis in hepatocellular carcinoma with methyl-C-11 choline: correlation with in vivo metabolic studies. J Nucl Med 2011;52:98–106.
23. Katz-Brull R, Margalit R, Degani H. Differential routing of choline in implanted breast cancer and normal organs. Magn Reson Med 2001;46:31–38.
24. Hara T, Kosaka N, Shinoura N, Kondo T. PET imaging of brain tumor with [methyl-C-11]choline. J Nucl Med 1997;38:842–847.
25. Moseley RH, Takeda H, Zugger LJ. Choline transport in rat liver basolateral plasma membrane vesicles. Hepatology 1996;24:192–197.
26. Antai AB, Eyong EU, Eteng MU, Itam EH, Eko ME, Ita SO. Serum protein and enzyme levels in rats following administration of ethanolic leaf extract of Ageratum conyzoides (goat weed). Niger J Physiol Sci 2009;24:117–120.
27. Plathow C, Weber WA. Tumor cell metabolism imaging. J Nucl Med 2008;49:43–63.
28. Allen DD, Smith QR. Characterization of the blood-brain barrier choline transporter using the in situ rat brain perfusion technique. J Neurochem 2001;76:1032–1041.
29. Muller SA, Holzapfel K, Seidl C, Treiber U, Krause BJ, Senekowitsch-Schmidtke R. Characterization of choline uptake in prostate cancer cells following bicalutamide and docetaxel treatment. Eur J Nuc Med Mol Imaging 2009;36:1434–1442.
30. Smith G, Zhao YJ, Leyton J, et al. Radiosynthesis and preclinical evaluation of [F-18]fluoro-[1,2-H-2(4)]choline. Nucl Med Biol 2011;38:39–51.
31. Hara T, Kondo T, Hara T, Kosaka N. Use of F-18-choline and C-11-choline as contrast agents in positron emission tomography imaging-guided stereotactic biopsy sampling of gliomas. J Neurosurg 2003;99:474–479.
32. Agut J, Font E, Sacristan A, Ortiz JA. Dissimilar effects in acute toxicity studies of CDP-choline and choline. Arzneimittelforschung 1983;33:1016–1018.
33. Allouche-Arnon H, Wade T, Waldner LF, et al. In vivo magnetic resonance imaging of glucose - initial experience. Contrast Media Mol Imaging 2013;8:72–82.